Modeling and Energy Evaluation of Small Convertible UAVs

Duc Kien Phung, Pascal Morin

Modeling and Energy Evaluation of Small Convertible UAVs ⋆

Duc-Kien Phung * **Pascal Morin** *

* *Institut des Systèmes Intelligents et de Robotique, Université Pierre et Marie Curie, Paris, 75252, France (e-mail: {phung,morin}@isir.upmc.fr).*

Abstract: This paper proposes a modeling of the energy consumption of a class of small convertible VTOL-UAVs (Vertical Take-Off and Landing Unmanned Aerial Vehicles). We consider systems composed of a set of coplanar propellers for propulsion and wing(s) to improve energy efficiency. Aerodynamics of propellers is modeled from standard momentum and blade element theories. In order to obtain simple closed-form expressions, modeling simplifications are made and a six-parameter-analytical model is proposed. The model parameters are identified from the experimental data reported in the literature. As for the wing(s), a NACA profile is selected and an approximate model of lift and drag coefficients over the entire flight domain is defined. Based on these models, the calculation of energy consumption reduces to solving a minimization problem in two variables. As an application, we compare the energy consumption of different convertible structures in the horizontal-flight range of $[0, 20]$m/s. This comparison provides useful guidelines for both conception and control of convertible UAVs.

Keywords: modeling, energy, convertible, UAV, VTOL

1. INTRODUCTION

Vertical Take-Off and Landing - Unmanned Aerial Vehicles (VTOL-UAVs) are becoming increasingly important in civilian and military applications. Recent years have seen the emergence of small and low-cost VTOL-UAVs (a few kilograms and a few thousand dollars), like the popular quadrotor (Hamel et al., 2002; Hoffmann et al., 2007; Guenard, 2007; Pounds et al., 2010). The quadrotor is optimized for hover flight but its energy efficiency in cruising flight is generally poor. This limits the duration of a typical mission. For example, a quadrotor like the one described in the article by Aleksandrov and Penkov (2012) has dimensions 500 mm × 500 mm × 90 mm and its weight is 1.4 kg. Its battery capacity is 4900mAh at 11.1 V, the power of all four motors is 130 W, and it can fly for only 20 min. Convertible aerial vehicles, which use both fixed and rotary wing(s), constitute an alternative to the quadrotor with the goal of improving energy efficiency in cruising flight. The versatility of these aerial vehicles explains the growing interest in the modeling and control of such systems (Pflimlin, 2006; Naldi and Marconi, 2010; Bhanja C. et al., 2012). To our knowledge there are few works on the energy consumption of these systems despite the fact that energy efficiency is the main incentive for using a convertible VTOL-UAV in place of a more classical structure. There exists a large literature on the modeling and energy consumption of helicopters (Stepniewski and Keys, 1979; Newman, 1994; Bramwell et al., 2001). In these references, momentum and blade element theories are the main ingredients for propellers modeling and these tools can be used for convertible UAVs as well. However, the case of small convertible UAVs needs to be specifically addressed. First, lift forces acting on the wing(s) of a convertible vehicle can be important and must be taken into account in the analysis since they modify substantially the thrust necessary to sustain the vehicle's weight and impact on the vehicle's orientation. By contrast, energy evaluation for helicopters typically assumes that the propellers must sustain the vehicle's weight. Then, the power decomposition in term of induced power, profile power, and parasite power is always used for helicopters but its justification for convertible vehicles is not clear due to the aforementioned large variations of thrust and vehicle orientation. Also, we are interested here by fixed-pitch propellers so that changes in thrust are accomplished by changing the propeller's rotational velocity. This contrasts with the case of helicopters. For example, Newman (1994) presents the procedure to calculate the energy of helicopters while assuming that the propeller's velocity (blade tip velocity) is constant. Finally, one must also account for a degradation in performance of propellers at low Reynolds number compared to larger propellers for full-scale airplanes, as mentioned by Brandt and Selig (2011). Focusing on small VTOL-UAVs with fixed-pitch propellers (like the classical quadrotor), Aleksandrov and Penkov (2012) compare the energy consumption of vehicles with different numbers of rotors. The power calculation is very simplified and does not take into account the influence of the flying speed on the induced velocity and rotor drag. Furthermore, the UAVs considered in Aleksandrov and Penkov (2012) are multi-rotor systems but they do not include wing(s). Hoffmann et al. (2007) take into account the effect of thrust change in forward flight but the rotor drag is not taken into account and, like in Aleksandrov and Penkov (2012), the considered systems are not convertible.

⋆ This work is supported by the "Chaire d'excellence en Robotique RTE-UPMC".

The objective of this work is to propose an approach for the energy evaluation of a class of convertible VTOL-UAVs. The approach consists of three steps. The first step concerns the aerodynamic modeling of propellers and wing(s). For propellers, the modeling relies on classical methods from momentum and blade element theories, as found in helicopter literature (Newman, 1994; Stepniewski and Keys, 1979; Bramwell et al., 2001). In particular, a simplified six-parameter-analytical model is proposed and model parameters are identified from experimental data reported in literature. Concerning the wing(s) a recently proposed analytical model of aerodynamic forces acting on the wing for possible large angles of attack is used (Pucci et al., 2011). The second step consists in determining propellers' speed and UAV's orientation for a given flight speed. The third step is a straightforward calculation of the power and energy consumption from the propellers' speed and the torque needed to drive each propeller. Behind the fact that lift forces are here explicitly taken into account, this approach also differs from the standard approach used for helicopters. Indeed, we do not rely on the commonly used (but rarely justified) "superposition principle" to express power as the sum of induced, profile, and parasite power. Application of the present work essentially concerns convertible UAVs' design and control. Concerning the design issue, we compare some convertible structures and evaluate the impact of the inclination angle of the wing(s) with respect to the propellers' plane on the energy consumption at different flying velocities. As for the control issue, it is not addressed in this paper but the energy evaluation provides useful guidelines for the control of wing(s)' angles of attack.

The paper is organized as follows. Section 2 provides a preliminary description of the problem together with a sketch of the modeling approach. The proposed model is detailed in section 3. Using momentum and blade element theories, a simplified analytical model to compute propellers' power is proposed and the model parameters are identified from experimental data. By completing this model with an aerodynamic model for the wing(s), one can then determine the energy consumption for a given airspeed. Based on this modeling, we compare in Section 4 the energy consumption of different UAV configurations. Section 5 provides a brief summary of the paper and perspectives.

2. PRELIMINARIES AND MODELING APPROACH

We consider a VTOL-UAV composed of a set of N coplanar propellers of same size and characteristics and a main body, as depicted in vertical projection on the left part of fig. 1. The following notation is used: [1]

- $\mathcal{I} = \{O, \boldsymbol{i_0}, \boldsymbol{j_0}, \boldsymbol{k_0}\}$ is an inertial frame with $\boldsymbol{k_0}$ pointing downward. This choice is consistent with the common use of NED (North-East-Down) frames in aeronautics.
- $\mathcal{B} = \{G, \boldsymbol{i}, \boldsymbol{j}, \boldsymbol{k}\}$ denotes a body frame with G the vehicle's center of mass and $\{\boldsymbol{i}, \boldsymbol{j}, \boldsymbol{k}\}$ coinciding with $\{\boldsymbol{i_0}, \boldsymbol{j_0}, \boldsymbol{k_0}\}$ when the vehicle is in hover. The plane $(G, \boldsymbol{i}, \boldsymbol{j})$ also coincides with the propellers' plane.
- $\boldsymbol{\dot{x}_a}$ denotes the linear air-velocity of the UAV and the vector of coordinates of $\boldsymbol{\dot{x}_a}$ in $\mathcal{I}$ is denoted as $\dot{x}_a$, i.e. $\boldsymbol{\dot{x}_a} = \dot{x}_{a,1}\boldsymbol{i_0} + \dot{x}_{a,2}\boldsymbol{j_0} + \dot{x}_{a,3}\boldsymbol{k_0}$.

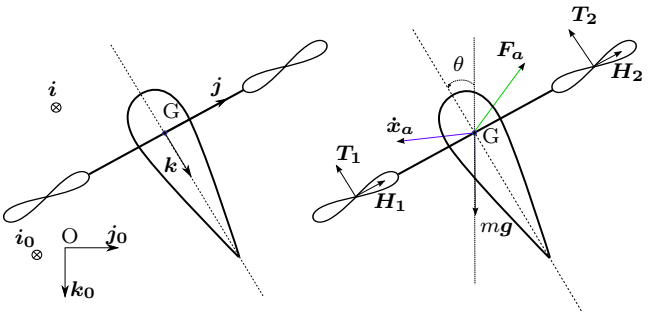

Fig. 1. 2-D Model

Assumptions: Throughout the paper we focus on a 2D motion [2] in the plane $(O, \boldsymbol{j_0}, \boldsymbol{k_0}) = (G, \boldsymbol{j}, \boldsymbol{k})$ spanned by the gravity vector and the UAV's linear velocity vector. It is assumed that the vehicle moves at zero angular velocity and constant linear velocity. It is also assumed that all aerodynamic forces acting on the UAV are tangent to the motion plane $(O, \boldsymbol{j_0}, \boldsymbol{k_0})$. This requires in particular the wind velocity to be parallel to the plane $(O, \boldsymbol{j_0}, \boldsymbol{k_0})$.

From these assumptions, the vehicle's orientation is fully determined by the angle θ [3] between $\boldsymbol{k_0}$ and $\boldsymbol{k}$. The following forces, orthogonal to $\boldsymbol{i_0}$, act on the vehicle (see the right part of fig. 1):

- The vehicle's weight $\boldsymbol{W} = mg\,\boldsymbol{k_0}$ with m the vehicle's mass and g the gravity constant;
- The aerodynamic force $\boldsymbol{F_a} = F_{a,2}\,\boldsymbol{j_0} + F_{a,3}\,\boldsymbol{k_0}$ acting on the vehicle's main body;
- The thrust forces $\boldsymbol{T_i} = -T_i\,\boldsymbol{k}$ $(i = 1, \cdots, N)$ acting on the propellers, with $T_i \geq 0$ the intensities of these forces;
- The in-plane forces $\boldsymbol{H_i} = H_i\,\boldsymbol{j}$ $(i = 1, \cdots, N)$ acting on the propellers, with $H_i \geq 0$ the intensities of these forces.

Since the vehicle moves at constant linear velocity, Newton's law implies that the following two relations are satisfied: [4]

$$\sum_{i=1}^{N} T_i = (mg + F_{a,3})c_\theta - F_{a,2}s_\theta \tag{1}$$

$$\sum_{i=1}^{N} H_i = -F_{a,2}c_\theta - (mg + F_{a,3})s_\theta \tag{2}$$

In order to satisfy the assumption of motion with zero angular velocity, the moment of external forces must also be zero. On a multi-rotor system this is typically achieved by a proper choice of T_i, consistent with Eq. (1). For

[1] Throughout the paper, bold letters are used for vectors in Euclidean space whereas ordinary letters are used for coordinates of these vectors in a basis.

[2] This work can be extended to the general 3D case, for example to take into account lateral forces induced by a non-zero side-slip angle, at the expense of a notably more complicated exposition.

[3] Note that θ is measured positively from $\boldsymbol{j_0}$ to $\boldsymbol{k_0}$, i.e. θ in fig. 1 is negative.

[4] The following shorthand notation for trigonometric function is used: $c_\theta \triangleq \cos\theta, \quad s_\theta \triangleq \sin\theta$.

simplicity we assume that this property is satisfied with $T_i = T, \forall i$, i.e. all propellers deliver the same thrust. This is usually satisfied with a good degree of accuracy for a well-built quadrotor. Then, Eq. (1) and Eq. (2) reduce to:

$$T = \frac{1}{N}\Big[(mg + F_{a,3})c_\theta - F_{a,2}s_\theta\Big] \quad (3)$$

$$H = \frac{1}{N}\Big[- F_{a,2}c_\theta - (mg + F_{a,3})s_\theta\Big] \quad (4)$$

with T and H the respective thrust and in-plane force intensities on each propeller.

The approach used to model the energy consumption proceeds as follows.

(1) **Analytic modeling of aerodynamic forces:** Using momentum and blade element theories, analytical models of T, H, and the torque Q needed to drive each propeller are derived:

$$\begin{cases} T &= f_T(\theta, \dot{x}_a, \varpi, \nu_{ind}) \\ H &= f_H(\theta, \dot{x}_a, \varpi, \nu_{ind}) \\ Q &= f_Q(\theta, \dot{x}_a, \varpi, \nu_{ind}) \end{cases} \quad (5)$$

where ϖ is the rotational speed of a propeller and the so-called "induced velocity" ν_{ind} is the solution of an implicit analytic equation:

$$f_\nu(\theta, \dot{x}_a, T, \nu_{ind}) = 0 \quad (6)$$

As for the modeling of aerodynamic forces acting on the wing(s), an analytical model recently proposed in Pucci et al. (2011) is used:

$$F_a = f_a(\theta, \dot{x}_a) \quad (7)$$

where the function f_a will be specified further. Note that, by assuming F_a does not depend on ϖ and ν_{ind}, we implicitly neglect interactions between the flow induced by the propellers and the flow along the wing(s).

(2) **Determination of the orientation equilibrium and propellers' speed:** Using the fact that the function f_T is invertible with respect to $\varpi \geq 0$, ϖ can be expressed as a function of $\theta, \dot{x}_a, T$, and ν_{ind}:

$$\varpi = f_\varpi(\theta, \dot{x}_a, T, \nu_{ind}) \quad (8)$$

where the function f_ϖ is obtained by inversion of f_T with respect to ϖ. From Eq. (5), (7), and (8), Eq. (3) and Eq. (4) can be written as:

$$T = \frac{1}{N}\Big[\big(mg + f_{a,3}(\theta, \dot{x}_a)\big)c_\theta - f_{a,2}(\theta, \dot{x}_a)s_\theta\Big] \quad (9)$$

$$f_H\Big(\theta, \dot{x}_a, f_\varpi(\theta, \dot{x}_a, T, \nu_{ind}), \nu_{ind}\Big) = \frac{1}{N}\Big[- f_{a,2}(\theta, \dot{x}_a)c_\theta - \big(mg + f_{a,3}(\theta, \dot{x}_a)\big)s_\theta\Big] \quad (10)$$

Replacing T in Eq. (6) and Eq. (10) by the right-hand side of Eq. (9), one obtains two implicit equations in two unknowns θ and ν_{ind}. This system of equations is solved numerically to obtain the equilibrium orientation θ and the induced velocity ν_{ind}. The value of T is then given by Eq. (9) and the propeller speed ϖ by Eq. (8).

(3) **Energy consumption:** The torque Q is obtained directly from Eq. (5). This allows one to compute the power $P = NQ\varpi$ and subsequently the energy consumption.

Before proceeding with the details, a few remarks are necessary.

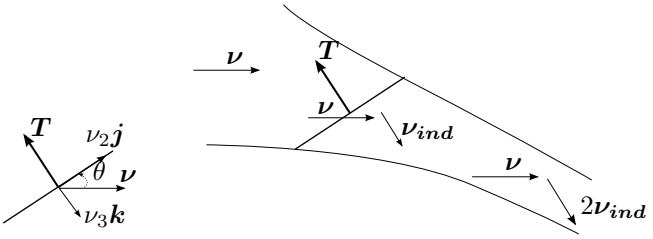

Fig. 2. Actuator disk streamtube in forward flight (adapted from figure 5.1 page 64 in Newman, 1994)

i) The proposed approach can be simplified by neglecting the in-plane forces H_i which are typically small w.r.t. the aerodynamic forces acting on the wing. This corresponds to setting $H = 0$ in Eq. (4) (i.e. $f_H = 0$ in Eq. (10)). Then, θ is first determined by numerically solving Eq. (10) and ν_{ind} is determined next from Eq. (6) using expression Eq. (9) for T. In this way solving a system of two equations in two unknowns is reduced to solving independently two systems of one equation in one unknown.

ii) Concerning Step 2, there may exist several solutions $(\theta,\ \nu_{ind})$ to Eq. (10). In particular, even when the in-plane force H is neglected, strong lift forces and the associated stall phenomenon can lead to several orientation equilibriums for a given airspeed $\dot{x}_a$. The reader is referred to Pucci (2012) for more details on this issue. In practice, being essentially interested in minimizing the energy consumption, only the equilibrium orientation associated with the minimum energy consumption is of interest.

3. PROPOSED MODEL

We now detail the modeling procedure sketched in the previous section. The main objective is to determine the functions f_T, f_H, f_Q, f_ν, and f_a that can approximate the associated physical quantities with good accuracy. The analytical model for the propellers is presented hereafter.

3.1 Analytical Model for the Propellers

Momentum theory is used to obtain the velocity induced by the propeller (Newman, 1994). Assume that the propeller is flying at (air-)velocity $\dot{\boldsymbol{x}}_{\boldsymbol{a}}$. The diagram of the flow streamtube is illustrated in fig. 2. The flow velocity is $\boldsymbol{\nu} = -\dot{\boldsymbol{x}}_{\boldsymbol{a}}$. The vector $\boldsymbol{\nu}$ is decomposed along the vectors $\boldsymbol{j}$ and $\boldsymbol{k}$ attached to the propeller: $\boldsymbol{\nu} = \nu_2\boldsymbol{j} + \nu_3\boldsymbol{k}$. The velocity intensity of the total flow across the disk is thus: $\nu' = \sqrt{\nu_2^2 + (\nu_3 + \nu_{ind})^2}$. The well-known Glauert's formula to find the induced velocity is:

$$\nu_{ind} - \frac{T}{2\rho A}\frac{1}{\sqrt{\nu_2^2 + (\nu_3 + \nu_{ind})^2}} = 0 \quad (11)$$

where ρ is the air density, $A = \pi R^2$ is the area swept by the propeller blades, and R is the propeller radius. Expressing ν in term of $\dot{x}_a$ and θ, i.e.

$$\nu_2 = -(\dot{x}_{a,2}c_\theta + \dot{x}_{a,3}s_\theta)\,, \quad \nu_3 = \dot{x}_{a,2}s_\theta - \dot{x}_{a,3}c_\theta$$

it follows from Eq. (11) that Eq. (6) is satisfied with:

$$f_\nu(\theta, \dot{x}_a, T, \nu_{ind}) = \nu_{ind} - \frac{T}{2\rho A\sqrt{|\dot{x}_a|^2 + \nu_{ind}^2 + 2\nu_{ind}(\dot{x}_{a,2}s_\theta - \dot{x}_{a,3}c_\theta)}} \quad (12)$$

Now we review some aspects of blade element theory to develop our modeling expressions. In order to obtain simple closed-form expressions, modeling assumptions are made as follows:

- The chord length and the pitch angle of the propeller blades vary along the blade. It is shown in Newman (1994) that one can take the chord length c_P and the pitch angle θ_P at 75% radius to have good average values. This amounts to assuming that the propeller blade has rectangular shape with width c_P and fixed pitch θ_P.
- It is assumed that the rotational speed of the rotor is high w.r.t. the air-velocity ($\varpi \in [3000, 6000]$ RPM at normal operating conditions). This allows us to neglect the reverse flow region and assume that the angle of attack α_P of the blade is always small.
- The tip loss factor (Bramwell et al., 2001), which accounts for only about 5% thrust loss, is ignored in our modeling.

To non-dimensionalize the equations, the following notation is used with the rotor tip speed $\nu_T = \varpi R$:

$$\bar{\nu} = \frac{\nu}{\nu_T}, \quad \bar{\nu}_2 = \frac{\nu_2}{\nu_T}, \quad \bar{\nu}_3 = \frac{\nu_3}{\nu_T}, \quad \bar{\nu}_{3,ind} = \frac{\nu_3 + \nu_{ind}}{\nu_T}$$

The blade lift coefficient is modeled as a linear function of the blade's angle of attack α_P:

$$C_{LP}(\alpha_P) = C_{L0} + a\alpha_P \tag{13}$$

where C_{L0} is lift coefficient at zero angle attack and a is the lift curve slope. This model takes into account the lift coefficient at zero angle attack, which can modify the blade lift force significantly because propeller blades usually have non-symmetric cross-section airfoil. By contrast, most helicopter's models like in Bramwell et al. (2001) do not include C_{L0}. The blade drag coefficient is modeled as a quadratic function of α_P:

$$C_{DP}(\alpha_P) = b_0 + b_1\alpha_P + b_2\alpha_P^2 \tag{14}$$

where b_i with $i \in \{0, 1, 2\}$ are constant values. Equation (14) gives a fairly accurate curve that models the parabolic evolution of drag coefficient in non-symmetric airfoil. For comparison, in almost every works on helicopter modelings (Stepniewski and Keys, 1979; Newman, 1994; Bramwell et al., 2001), C_{DP} is modeled as a simple constant. Based on classical blade element theory, [5] the thrust expression is:

$$T = \frac{\rho N_P c_P R}{4}\left[C_{Lt}\left(\frac{2}{3} + \bar{\nu}_2^2\right) - a\bar{\nu}_{3,ind}\right]\nu_T^2 \tag{15}$$

where $C_{Lt} = C_{L0} + a\theta_P$ is the value of the blade lift coefficient at the fixed pitch angle and N_P is the number of blades on a propeller. We can simplify Eq. (15) further by noting that $\bar{\nu}_2 = \nu_2/\nu_T$ is small in normal conditions since it is assumed that $|\nu_2| \in [0, 20]$ m/s, whereas ν_T is typically in the range $[60, 115]$ m/s and increases when $|\nu_2|$ increases. Typically $\bar{\nu}_2 \leq 0.2$ so that one can neglect the $\bar{\nu}_2^2$ term:

$$T = \frac{\rho N_P c_P R}{4}\left(\frac{2}{3}C_{Lt} - a\bar{\nu}_{3,ind}\right)\nu_T^2 \tag{16}$$

Let us define constants β_i with $i \in \{0, 1, 2\}$ as follows:

$$\begin{aligned}\beta_0 &= b_2 - a\\ \beta_1 &= C_{Lt} - 2\theta_P b_2 - b_1\\ \beta_2 &= b_2\theta_P^2 + b_1\theta_P + b_0\end{aligned} \tag{17}$$

Then, the in-plane drag force is: [5]

$$H = \frac{\rho N_P c_P R}{4}\bar{\nu}_2(\beta_1\bar{\nu}_{3,ind} + \beta_2)\nu_T^2 \tag{18}$$

Finally, the torque expression is: [5]

$$\begin{aligned}Q &= \frac{\rho N_P c_P R^2}{4}\left[\bar{\nu}_{3,ind}\left(\frac{2}{3}\beta_1 + \beta_0\bar{\nu}_{3,ind}\right) + \frac{\beta_2}{2}(1 + \bar{\nu}_2^2)\right]\nu_T^2\\ &\approx \frac{\rho N_P c_P R^2}{4}\left[\bar{\nu}_{3,ind}\left(\frac{2}{3}\beta_1 + \beta_0\bar{\nu}_{3,ind}\right) + \frac{\beta_2}{2}\right]\nu_T^2\end{aligned} \tag{19}$$

Our modeling equations are more general than the ones in Newman (1994) since we make use of more accurate model of the blade aerodynamic coefficients. From Eq. (16), (18), and (19), we can express T, H, Q as functions of θ, $\dot{x}_a$, ϖ, ν_{ind}. Therefore, Eq. (5) is satisfied with:

$$\begin{cases} f_T(\theta, \dot{x}_a, \varpi, \nu_{ind}) = \dfrac{\rho N_P c_P R^2}{4}\Big[\dfrac{2}{3}C_{Lt}R\varpi^2 \\ \qquad\qquad -a(\dot{x}_{a,2}s_\theta - \dot{x}_{a,3}c_\theta + \nu_{ind})\varpi\Big] \\ f_H(\theta, \dot{x}_a, \varpi, \nu_{ind}) = \dfrac{\rho N_P c_P R}{4}(\dot{x}_{a,2}c_\theta + \dot{x}_{a,3}s_\theta) \\ \qquad\qquad \Big[\beta_1(\dot{x}_{a,2}s_\theta - \dot{x}_{a,3}c_\theta + \nu_{ind}) + \beta_2 R\varpi\Big] \\ f_Q(\theta, \dot{x}_a, \varpi, \nu_{ind}) = \dfrac{\rho N_P c_P R^2}{4}\Big\{(\dot{x}_{a,2}s_\theta - \dot{x}_{a,3}c_\theta + \nu_{ind}) \\ \quad \Big[\dfrac{2}{3}\beta_1 R\varpi + \beta_0(\dot{x}_{a,2}s_\theta - \dot{x}_{a,3}c_\theta + \nu_{ind})\Big] + \beta_2 R^2\varpi^2\Big\} \end{cases} \tag{20}$$

3.2 Six-parameter Model and Identification

Let us recall the definitions of non-dimensional coefficients used for the characterization of propellers (see, e.g. Newman, 1994):

$$C_T \triangleq \frac{T}{\frac{1}{2}\rho A\nu_T^2}, \quad C_H \triangleq \frac{H}{\frac{1}{2}\rho A\nu_T^2}, \quad C_P = C_Q \triangleq \frac{Q}{\frac{1}{2}\rho AR\nu_T^2} \tag{21}$$

From Eq. (16) and Eq. (21),

$$C_T = \frac{s}{2}\left(\frac{2}{3}C_{Lt} - a\bar{\nu}_{3,ind}\right) \tag{22}$$

where s is the solidity of the propeller, which is the ratio of the area of the blades over the area of the propeller disk: $s = N_P c_P R/A$. From Eq. (18) and Eq. (21), the drag coefficient for H force is:

$$C_H = \frac{s\bar{\nu}_2}{2}(\beta_1\bar{\nu}_{3,ind} + \beta_2) \tag{23}$$

From Eq. (19) and Eq. (21), the power (torque) coefficient is:

$$C_P = C_Q = \frac{s}{2}\bar{\nu}_{3,ind}\left(\frac{2}{3}\beta_1 + \beta_0\bar{\nu}_{3,ind}\right) + \frac{s}{4}\beta_2 \tag{24}$$

The propeller power can be calculated from the power coefficient and the tip velocity: $P = \frac{1}{2}\rho AC_P\nu_T^3/\eta_M$ where the factor η_M is introduced in this expression as motor efficiency. In addition, we define the axial advance ratio as the ratio of the vehicle air speed along the thrust (axial) direction over the tip velocity: $J_a = \pi|\nu_3|/\nu_T$. The efficiency of a propeller is defined as: $\eta_P = J_a C_T/C_P$.

[5] The calculation steps, although more general, are very similar to the ones in Newman (1994) Chapter 5.

The model defined by equations (22), (23), and (24) depends on six parameters associated with the propellers' blades:

- a geometric parameter: s
- five coefficients related to aerodynamic parameters: C_{Lt}, a, $\beta_0, \beta_1, \beta_2$.

The geometric parameter s (and θ_P) can be easily obtained from direct measurements on the blade (or from data available by manufacturers) and one is left with the determination of five parameters characterizing the blade aerodynamic coefficients. These parameters are usually not available by the propellers manufacturers. It is possible to manually measure each blade profile at different radius stations on the blade, and then use a vortex panel program like XFoil (Drela, 2008) (see Moffitt et al., 2008 for more information on the procedure). This is complicated and time consuming, however, and the result may be significantly affected by measurement errors. A better solution, when possible, is to use five thrust and torque (or power) measurements. One essentially needs five measurements. Two of them can be easily obtained from thrust and torque measurements on a static test bench (corresponding to stationary flight). This can be complemented by three measurements in axial flight. We illustrate this on the APC 11x4.7 propeller. [6] For simplicity and consistence, we make use of UIUC wind tunnel measurements to identify the five aerodynamic coefficients. It is worth noting that increasing the Reynolds number improves propeller performance, as mentioned in many studies, including Brandt and Selig (2011). We do not try to model this effect here because propellers typically operate relatively close to a given angular speed. On the thrust coefficient C_T versus the axial advance ratio J_a curve, at each angular speed ϖ, 2 points are selected: a point at minimum J_a and another point at maximum J_a. Then from Eq. (22), we can easily solve 2 equations for 2 unknowns C_{L0} and a. For each rotor angular speed ϖ, we obtain a pair of C_{L0} and a. For example, $C_{L0} = [0.418; 0.457; 0.499; 0.540]$ at corresponding $\varpi = [3000; 4000; 5000; 6000]$. We can take the average value $C_{L0} = 0.478$ for the mean value of lift coefficient at zero angle of attack at angular speed $\varpi \in [3000 - 6000]$. Similarly, using the power coefficient C_P versus the axial advance ratio J_a curve at each angular speed ϖ, taking 3 points (2 points at the extremes and 1 point in the middle), we can obtain the blade drag coefficients b_0, b_1, and b_2. The values of β_0, β_1, and β_2 are directly obtained from Eq. (17).

In order to validate our six-parameter-analytical model, we compare our result at rotor angular speed 6000 RPM with the manufacturer data, experimental data from literature, and a propeller calculation software called PropCalc (Schenk, 2012). Fig. 3 shows the axial efficiency of the propeller versus the axial advance ratio. Compared to UIUC data, PropCalc results shows similar trends but different values of the efficiency. APC data gives different trends for small advance ratio and significantly different amplitudes

[6] We have chosen the propeller APC SlowFlyer 11 × 4.7 for our application because among more than 140 propellers from the UIUC database (Brandt and Selig, 2012), it has one of the highest efficiency (max $\eta_P \approx 0.6$ for angular speed of 6000 RPM) and its efficient operating region falls in the suitable range of advance ratio $J_a \in [0.2, 0.5]$.

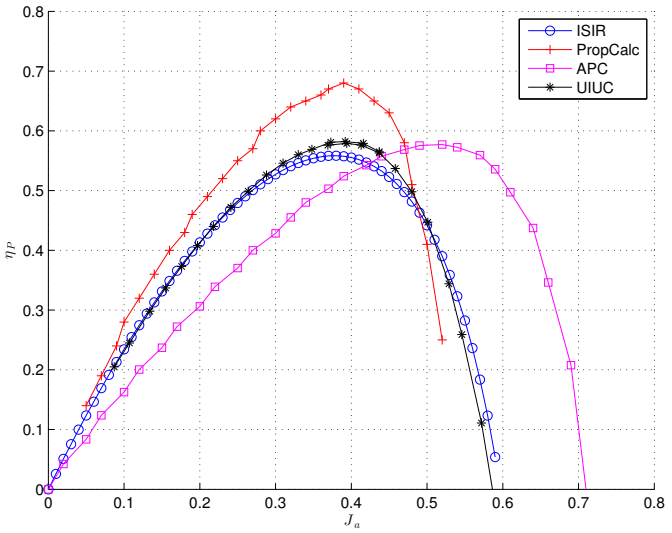

Fig. 3. Comparison of efficiencies of propeller APC SlowFlyer 11 × 4.7 vs the axial advance ratio - with rotor angular speed of 6000 RPM

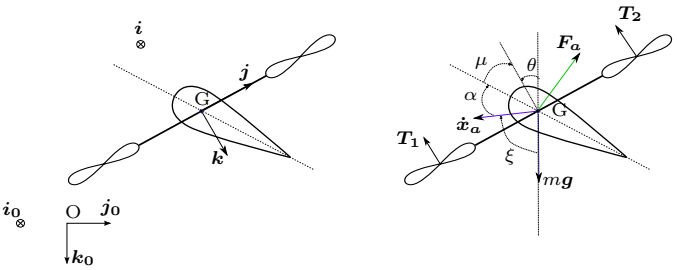

Fig. 4. 2-D Model

also. Compared to UIUC, this yields a different efficiency curve, shifted to the right. Finally, our model provides values close to UIUC. This is of course not a surprise since we made use of UIUC data to identify our model parameters. The only value of this comparison is to show that with very few measurements, we can obtain a model that fits well to measurements in a large range of advance ratio and angular speed (recall that the identification was not made from the 6000 RPM rotor angular speed here considered).

3.3 Analytical Model for the Main Body

The material of this section is based on Pucci et al. (2011) and Chapter 6 of Pucci (2013). The objective is to provide a model for the aerodynamic force $\boldsymbol{F}_a$ acting on the UAV's main body valid in a large operating domain. In fig. 4, we denote the angle between the zero-lift line and the propellers' thrust direction $\boldsymbol{k}$ as μ and the angle of the airspeed with respect to the fixed vertical direction $\boldsymbol{k_0}$ as $\xi(\dot{x}_a) = -\text{atan2}(\dot{x}_{a_2}, \dot{x}_{a_3})$. The angle of attack is then calculated as:

$$\alpha(\dot{x}_a, \theta, \mu) = \pi + \theta - \xi(\dot{x}_a) - \mu \tag{25}$$

According to Pucci et al. (2011), the model of aerodynamic forces $\boldsymbol{F_a}$ acting on the main body can be written as (assuming no lift on the main body):

$$\begin{aligned}\boldsymbol{F_a}(\alpha, \dot{\boldsymbol{x}}_{\boldsymbol{a}}) = & k_a |\dot{\boldsymbol{x}}_{\boldsymbol{a}}| \left[c_L(\alpha, \text{Re}) \dot{\boldsymbol{x}}_{\boldsymbol{a}}^{\perp} - c_D(\alpha, \text{Re}) \dot{\boldsymbol{x}}_{\boldsymbol{a}} \right] \\ & - k_{\text{para}} c_{\text{para}} |\dot{\boldsymbol{x}}_{\boldsymbol{a}}| \dot{\boldsymbol{x}}_{\boldsymbol{a}}\end{aligned} \tag{26}$$

with $\dot{\boldsymbol{x}}_{\boldsymbol{a}}^{\perp}$ obtained by rotating clockwise vector $\dot{\boldsymbol{x}}_{\boldsymbol{a}}$ by 90° in the plane $(O, \boldsymbol{j_0}, \boldsymbol{k_0})$, i.e. $\dot{\boldsymbol{x}}_{\boldsymbol{a}}^{\perp} = -\dot{x}_{a,3}\boldsymbol{j_0} + \dot{x}_{a,2}\boldsymbol{k_0}$. The first term in Eq. (26) represents the aerodynamic forces acting on the wing. One has $k_a = \rho\Sigma/2$ with Σ the area of the wing(s). The Reynolds number is $\mathrm{Re} = \rho|\dot{\boldsymbol{x}}_{\boldsymbol{a}}|c/\mu_v$ where c is the wing chord length and μ_v is air viscosity. The term $c_L(\alpha, \mathrm{Re})$ and $c_D(\alpha, \mathrm{Re}) > 0$ denote respectively the lift and drag aerodynamic coefficients of the wing. The second term in Eq. (26) represents the parasite drag acting on the UAV's main body (i.e. UAV's body except wing(s) and propellers). One has $k_{\mathrm{para}} = \rho\Sigma_{\mathrm{para}}/2$ with Σ_{para} the effective parasite area and c_{para} is a parasite constant.

For any fixed value of μ, Eq. (7) is satisfied by substituting Eq. (25) into Eq. (26):

$$\boldsymbol{f_a}(\theta, \dot{\boldsymbol{x}}_{\boldsymbol{a}}) = k_a|\dot{\boldsymbol{x}}_{\boldsymbol{a}}|\Big[c_L\big(\pi + \theta - \xi(\dot{x}_a) - \mu, |\dot{\boldsymbol{x}}_{\boldsymbol{a}}|\big)\dot{\boldsymbol{x}}_{\boldsymbol{a}}^{\perp} - c_D\big(\pi + \theta - \xi(\dot{x}_a) - \mu, |\dot{\boldsymbol{x}}_{\boldsymbol{a}}|\big)\dot{\boldsymbol{x}}_{\boldsymbol{a}}\Big] - k_{\mathrm{para}}c_{\mathrm{para}}|\dot{\boldsymbol{x}}_{\boldsymbol{a}}|\dot{\boldsymbol{x}}_{\boldsymbol{a}} \quad (27)$$

In this project, NACA0018 wing symmetric airfoil is selected for our model because of its moderate stall zone and rather high lift over drag ratio. By using a sigmoid function $\sigma\big(\alpha, \alpha_0(\mathrm{Re})\big) = (1+e^{\alpha-\alpha_0(\mathrm{Re})})^{-1} + (1+e^{180^\circ-\alpha-\alpha_0(\mathrm{Re})})^{-1}$ where $\alpha_0(\mathrm{Re})$ is the angle where the stall zone starts, the lift coefficient can be formulated as:

$$c_L(\alpha, \mathrm{Re}) = c_{2T}\sin(2\alpha)\sigma\big(\alpha, \alpha_0(\mathrm{Re})\big) + c_2\sin(2\alpha)\Big(1 - \sigma\big(\alpha, \alpha_0(\mathrm{Re})\big)\Big) \quad (28)$$

where c_{2T} is the lift constant for small angles of attack, c_2 is an "average" lift constant. The drag coefficient is modeled as:

$$c_D(\alpha, \mathrm{Re}) \approx c_D(\alpha) = c_1 + 2c_2\sin^2(\alpha) \quad (29)$$

The coefficients c_1 and c_2 are estimated following the method described in Pucci et al. (2011) for minimizing the cost function between the measured and estimated aerodynamic coefficients. c_{2T} is estimated by the linear interpolation of the lift curve at low angle of attack. Fig. 5 shows the comparison result between the modeled aerodynamic coefficients and those obtained from experiments. The modeled values are fairly close to the measured data. At the end of the stall region or at some high angle attack, the lift data are slightly different.

4. COMPARISON BETWEEN DIFFERENT UAV CONFIGURATIONS

Based on the previous modeling, in this section different UAV configurations are considered and evaluated in term of their energy consumption at constant velocity in horizontal cruising flight. We are primarily interested in evaluating the importance of the inclination angle μ between the propellers' plane and the wing (see fig. 4). All physical dimensions of the simulated UAVs are detailed in appendix A. As suggested in section 2, the energy consumption calculation in this section is simplified by neglecting the small in-plane force H.

4.1 Power Evaluation of Different UAV Configurations

Following the notation of fig. 4, five UAV configurations are considered:

(1) Case 1: μ minimizes the thrust force,

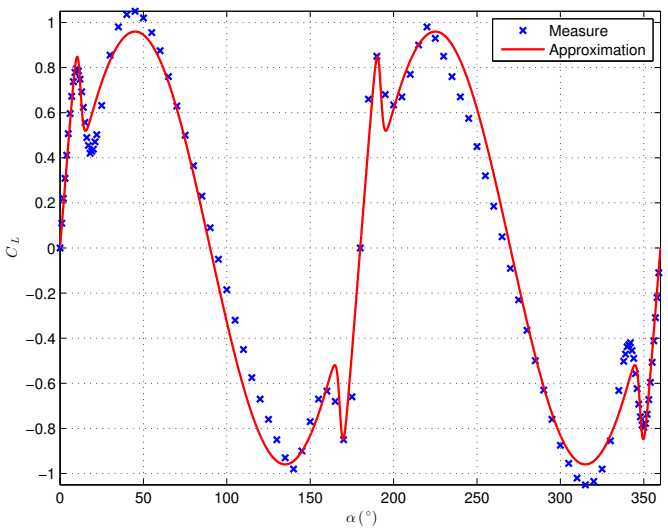

Fig. 5. Measured and modeled lift coefficients versus angle of attack at Re = 160000 for NACA0018 airfoil

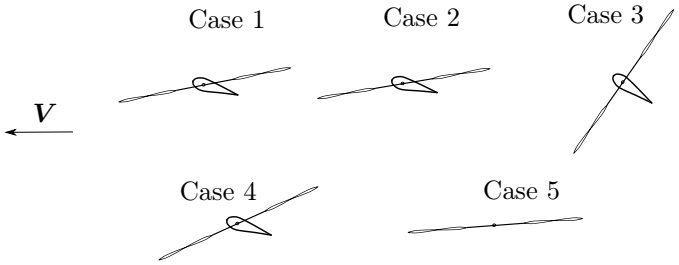

Fig. 6. The configuration in 5 cases for $V = 10$ m/s

(2) Case 2: μ minimizes the propellers power,
(3) Case 3: $\mu = 0$,
(4) Case 4: $\mu = \pi/4$,
(5) Case 5: no wing on the UAV (standard quadrotor).

Fig. 6 illustrates the UAV configuration of these five different cases at flying velocity $V = 10$ m/s. Fig. 7 shows the evolution of total power in these different cases. Case 1 (thrust minimization) power consumption is higher than Case 5 for speeds smaller than 8 m/s. In fact, at low speed Case 5 spends the least power because the UAV is evidently lighter without the wing(s). At speed $V \in [8, 13]$ m/s, Case 1 and Case 2 are very similar. Beyond that speed, Case 1 decreases rapidly in efficiency to approach the inefficient Case 3 ($\mu = 0$). At high speed indeed, the lift force in Case 1 is among the highest which translates into the lowest thrust force but the drag force is large. With large drag, the propellers incline at a large angle θ from the horizontal line. Generally when the magnitude of θ increases, the rotor angular speed ϖ increases fast. The propeller power is a function of the cube of the rotor angular speed, hence the variation of ϖ dictates the variation of P. Since ϖ in Case 1 is larger than in Case 2, the propeller power of the former case is also larger. We can conclude that optimization of the thrust is not always the best strategy to optimize the power. By contrast, for the optimal Case 2, the thrust is larger but the drag is kept at the lowest value. One could of course argue that the use of propellers better suited to high-speed flight could lead to better results at high speed for Case

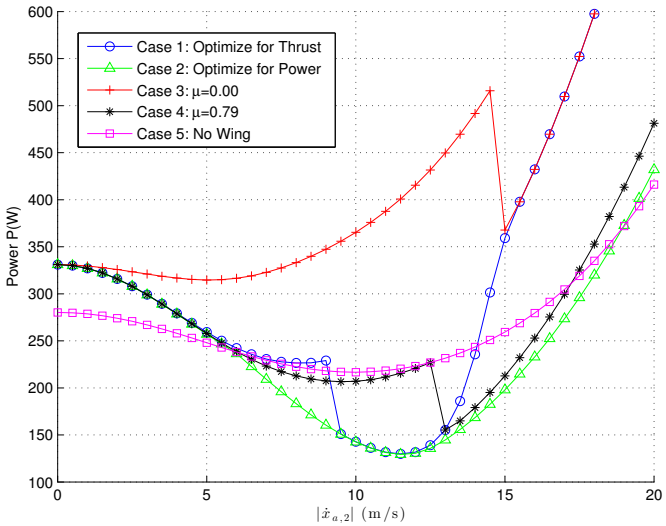

Fig. 7. The power comparison versus the speed

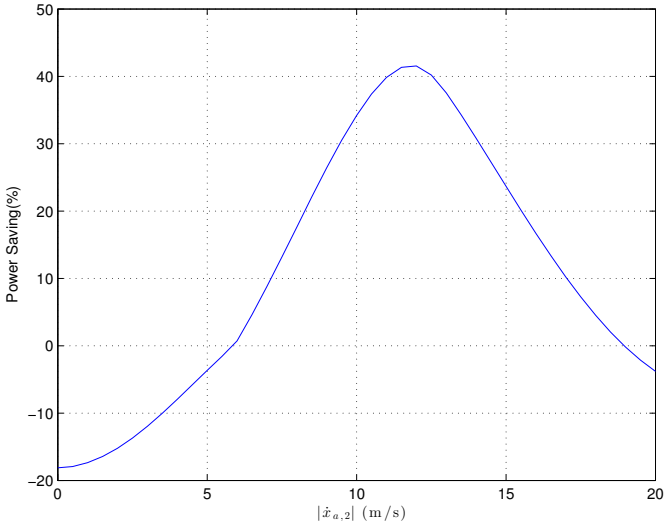

Fig. 8. The percentage of power saving versus the speed

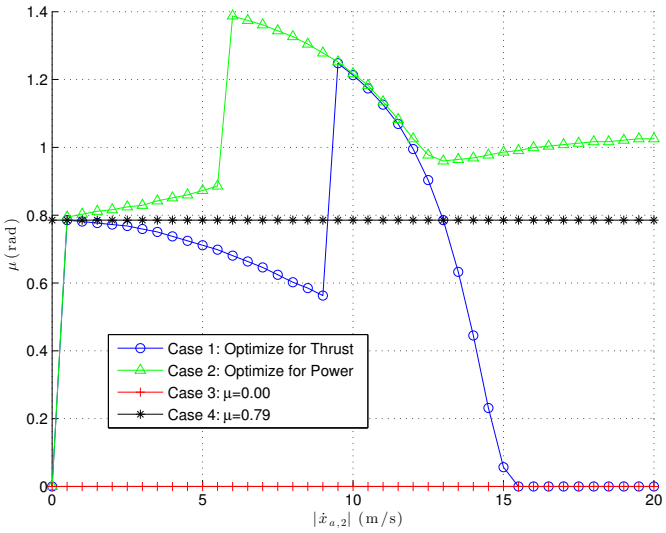

Fig. 9. The inclination angle μ versus the speed

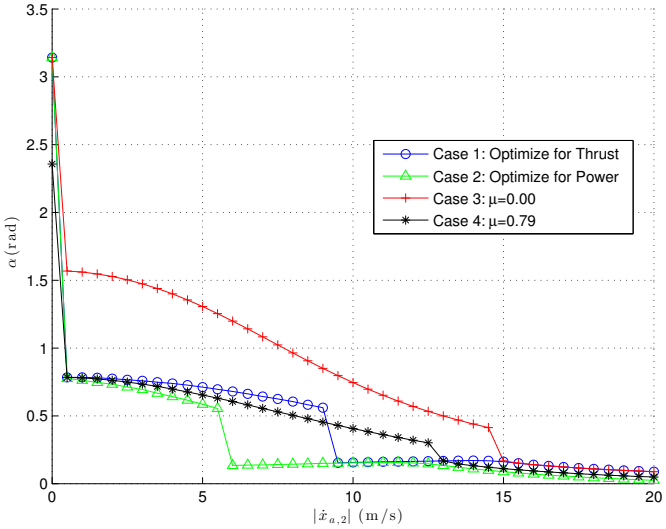

Fig. 10. The angle of attack α versus the speed

1. The choice of the propeller, however, is constrained by the requirement of good efficiency in stationary flight.

Concerning the optimal Case 2, fig. 8 shows the percentage of power saving w.r.t. Case 5 at different horizontal speeds. Adding the wing(s) significantly saves energy at "medium" speed. The configuration in Case 2 will save energy for a flying forward UAV at velocity between 6 and 19 m/s. The power saving is 42% at climax. One can note that the power saving varies with the forward speed in a "bell-curve" fashion: the gain of power is negative at very low speed, small at very high speed, but significant in between.

Case 3 is quite inefficient. The lift force acting on the wing is high. However, the drag force is also high. Therefore, the required thrust is one of the highest.

Finally, Case 4 is an example of a configuration with constant μ that achieves relatively satisfactory results. Although not as efficient as Case 2, it compares favorably with Case 5 in a significant range of velocities.

Fig. 9 shows the evolution of the angle μ for Cases 1 and 2. In Case 1, the angle μ is oriented to minimize the thrust, regardless of whether the drag is high. In contrast, in Case 2 the angle μ is oriented so as to reduce the thrust but also keep the drag at a small value. Fig. 10 demonstrates that at low speed, the wing(s) angles of attack α are different in the four considered cases. However, at high speed, the angles of attack in all cases are reduced to similar small values. At very high speed, even a small change in angle attack has great impact on the energy performance, as shown in fig. 7.

5. CONCLUSION

We have proposed a method to evaluate the energy consumption of VTOL-UAVs composed of coplanar propellers and a main body that may include wing(s). This method makes use of two analytical models of aerodynamic coefficients: a model of the propellers derived by combining momentum and blade element theories, and a model of the wing(s) recently proposed in the literature. From these models, energy evaluation is reduced to solving numerically a simple optimization problem. Energy consumption for five UAV configurations is then compared and ana-

lyzed in detail, allowing to determine the most efficient configuration in term of the inclination angle between the propellers' plane and the wing(s). It is shown that the optimal value of this angle depends on the airspeed and that adding wing(s) may be detrimental for energy consumption if this angle is poorly chosen. It is also verified that the configuration that minimizes the (propellers) thrust force does not necessarily minimizes energy. Indeed, adding wing(s) reduces the thrust force but increases the drag force, thereby yielding a larger inclination angle of the propellers' plane - which is not efficient from the energy point of view. Thus, the most efficient configuration is the one that provides the best trade-off between small thrust force and low drag force. Future work includes experiments to validate the proposed models on UAV prototypes, "energy efficient" control design, and studying the interaction between wing(s) and propellers.

REFERENCES

Aleksandrov, D., Penkov, I., 2012. Energy consumption of mini UAV helicopters with different number of rotors. In: 11th International Symposium "Topical Problems in the Field of Electrical and Power Engineering". pp. 259–262.

Bhanja C., A., Kulhare, A., Raina, G., May 2012. A generalized control method for a tilt-rotor UAV stabilization. In: 2012 IEEE International Conference on Cyber Technology in Automation, Control, and Intelligent Systems (CYBER). pp. 309–314.

Bramwell, A. R. S., Done, G. T. S., Balmford, D., Jan. 2001. Bramwell's Helicopter Dynamics, 2nd Edition. AIAA.

Brandt, J. B., Selig, M. S., 2011. Propeller performance data at low reynolds numbers. In: 49th AIAA Aerospace Sciences Meeting.

Brandt, J. B., Selig, M. S., 2012. UIUC propeller data site, http://www.ae.illinois.edu/m-selig/props/propDB.html.

Drela, M., 2008. XFoil subsonic airfoil development system, http://web.mit.edu/drela/Public/web/xfoil/.

Guenard, N., 2007. Optimisation et implementation de lois de commande embarquees pour la teleoperation de micro drones aeriens "X4-flyer". Ph.D. thesis, Universite Nice Sophia Antipolis.

Hamel, T., Mahony, R., Lozano, R., Ostrowski, J., 2002. Dynamic modelling and configuration stabilization for an x4-flyer. In: 15th Triennial World Congress, International Federation of Automatic Control.

Hoffmann, G. M., Huang, H., Waslander, S. L., Tomlin, C. J., 2007. Quadrotor helicopter flight dynamics and control: Theory and experiment. In: Proceedings of the AIAA guidance, navigation, and control conference. Vol. 4. p. 44.

Moffitt, B., Bradley, T., Parekh, D. E., Mavris, D., 2008. Validation of vortex propeller theory for UAV design with uncertainty analysis. In: AIAA.

Naldi, R., Marconi, L., Dec. 2010. On robust transition maneuvers for a class of tail-sitter vehicles. In: 2010 49th IEEE Conference on Decision and Control (CDC). pp. 358–363.

Newman, S., Apr. 1994. Foundations of Helicopter Flight. A Butterworth-Heinemann Title.

Pflimlin, J. M., 2006. Commande d'un minidrone à hélice carénée : De la stabilisation dans le vent à la navigation autonome. Ph.D. thesis, LAAS-CNRS.

Pounds, P., Mahony, R., Corke, P., Jul. 2010. Modelling and control of a large quadrotor robot. Control Engineering Practice 18 (7), 691–699.

Pucci, D., 2012. Flight dynamics and control in relation to stall. In: American Control Conference (ACC), 2012. pp. 118–124.

Pucci, D., 2013. Toward a unified approach for the control of aerial vehicles. Ph.D. thesis, Université de Nice Sophia-Antipolis.

Pucci, D., Hamel, T., Morin, P., Samson, C., 2011. Nonlinear control of PVTOL vehicles subjected to drag and lift. In: IEEE Decision and Control and European Control Conference. pp. 6177–6183.

Schenk, H., 2012. PropCalc - propeller calculator software, http://www.drivecalc.de/PropCalc/index.html.

Stepniewski, W. Z., Keys, C. N., 1979. Rotary-Wing Aerodynamics. Dover Publ.

Appendix A. SIMULATED MODEL

The physical dimensions of the UAV are as follows:

- wing chord length $c = 0.15$ m,
- wing(s) area $\Sigma = 0.21$ m^2,
- wing density $\rho_2 = 30$ kg/m^3 (EEP Foam 1.9),
- mass of the wing(s), the actuated servo(s), and linkage(s) to rotate the wing(s) $m_2 = \rho_2\Sigma(18\%c) + 0.1 = 0.27$ kg,
- mass of the UAV except the wing(s) $m_1 = 2.3$ kg,
- total mass of the UAV $m = m_1 + m_2 = 2.57$ kg.

The aerodynamic parameters of NACA0018 wing(s):

- drag constant $c_1 = 0.0128$,
- average lift constant $c_2 = 0.9595$,
- high lift constant $c_{2T} = 2.6749$,

The propellers chosen are APC SlowFlyer 11×4.7, which have the following parameters:

- number of propellers $N = 4$,
- number of blades per propeller $N_P = 2$,
- propeller radius $R = 0.1397$ m,
- propeller area $A = \pi R^2 = 0.061$ m^2,
- mean chord of a propeller blade at 75% radius $c_P = 0.028$ m,
- solidity of the propeller $s = N_P c_P R/A = 0.127$,
- pitch angle at 75% radius of the propeller blade $\theta_P = 0.1794$ rad,
- blade aerodynamic coefficients $[C_{L0}, a, b_0, b_1, b_2] = [0.48, 4.53, 0.02, 0.02, 2.21]$.

The standard constants are:

- air density $\rho = 1.225$ kg/m^3,
- air viscosity $\mu_v = 1.789 \times 10^{-5}$,
- gravity constant $g = 9.8$ m/s^2.

The parasite drag coefficient is $c_{\text{para}} = 0.4$ and the effective parasite drag area is $\Sigma_{\text{para}} = 0.1$ m^2. The propeller motor efficiency is assumed to be $\eta_M = 0.7$.